

# Scanning Tunneling Microscopy for Metal Deposition Studies

by D. M. Kolb and M. A. Schneeweiss

**E**lectrolytic metal deposition, particularly from aqueous solution, provides the basis for a number of indispensable industrial applications such as metal winning and refining, metal plating for corrosion protection, and surface finishing. Circuitboard manufacturing in microelectronics, in particular, has renewed interest in the research of metal deposition. In addition to its industrial significance, electrodeposition is also of principal interest in regard to its fundamentals, such as, the investigation of electrocrystallization phenomena.<sup>1</sup>

Electrochemical studies have in most cases concentrated on the very initial stages of metal deposition comprising the nucleation and growth of small clusters. These very first steps in the formation of any metal coating have an immediate impact on the structure and overall appearance of the emerging overlayer.

So far, the initial stages have been monitored by classical electrochemical techniques, such as current transients to determine the nucleation behavior,<sup>2</sup> or by optical methods (e.g. by reflectance spectroscopy<sup>3</sup> or light microscopy<sup>4</sup>) to study the morphology of the deposit. The invention of the scanning tunneling microscope (STM) gave a new and powerful tool to electrochemists<sup>5</sup> that has opened up new pathways to structure information of hitherto unprecedented detail.

## A New Tool

STM allows one to image electrode surfaces in situ, i.e. in an electrochemical cell under operating conditions, in real space and real time and - provided single crystal surfaces are used - with atomic scale resolution.<sup>6,7</sup> The operating principle of an STM (see Fig. 1) is relatively simple (which is often true for really great inventions). A fine metal tip, usually prepared by electrochemical etching of an appropriate

wire, is brought close to the surface under study and a voltage is applied between tip and substrate. At a distance of about 0.5-1.0 nm, electrons tunnel from one side to the other. The resulting tunneling current  $I_T$  depends sensitively on the tunneling distance  $s$ :

$$I_T \propto U_T \exp(-\text{const} \cdot \phi_T^{0.5} \cdot s)$$

where  $U_T$  is the tunneling voltage,  $\phi_T$  the tunnel barrier, and  $\text{const}=10.25 \text{ nm}^{-1}(\text{eV})^{-1/2}$  if  $\phi$  is given in eV and  $s$  in nm. For metal/electrolyte interfaces,  $\phi_T$  has a value of about 1.5 eV. In the most usual mode of operation, the tip is scanned across the surface with the tunneling current  $I_T$  (and thus the distance  $s$  between tip and surface) kept constant via a feedback circuit. Consequently, any height variation in the surface topography is directly reflected in the movement of the tip normal to the surface. Systematic mapping of the scanned area occurs by recording a grid of information line by line. The diminutive lateral and vertical motions of the tip are realized by the use of piezoelectric ceramics as actuators.

The major adaptation necessary for in situ investigations of electrochemical processes is the use of a bipotentiostat, which allows the control of the potentials of tip and sample (i.e. working electrode) independently of each other versus a reference electrode. Another seemingly small yet crucial challenge was the coating of the metal tip (except for the last few  $\mu\text{m}$ ) with inert material to such an extent that any residual faradaic currents at the tip/electrolyte interface are small compared to the tunneling current. This has been realized with the help of a number of materials, such as inert wax<sup>7</sup> or electrodeposition paint.<sup>8</sup>

## Underpotential Deposition

In many cases, the deposition of metal on a foreign substrate rather than

on a surface of its own kind is of interest. If the substrate metal is more noble than the metal to be deposited, it is frequently observed that metal deposition starts in a potential region positive of the respective Nernst potential by forming a monolayer. This apparent violation of Nernst's law simply reflects the fact that the bond between metal and substrate is stronger than that between the adatoms of the deposited metal and hence the deposit spreads over the substrate.<sup>9</sup> Deposition of the second and subsequent layers then usually requires an overpotential, i.e. a value markedly negative of the Nernst potential, although several exceptions to this rule are known. Underpotential deposition (UPD), i.e. deposition positive of the Nernst potential as described above, is most conveniently demonstrated in cyclic voltammetry, where the monolayer formation is clearly visible as a deposition current and from which adlayer coverages and free adsorption enthalpies can be derived. We note that despite the similarities of the technical terms *over-* and *underpotential* deposition, their origin is vastly different: while *overpotential* deposition occurs due to purely kinetic reasons (e.g. nucleation overpotential), *underpotential* deposition results from a higher interaction energy with the substrate and is often treated as an adsorption process. From cyclic voltammograms which often show a pronounced multi-peak structure, it had been inferred that metal adatoms deposited at underpotentials form ordered structures if atomically flat single-crystal surfaces are employed.<sup>10,11</sup>

One of the most thoroughly studied systems is Cu UPD on Au(111) in sulfuric acid solution. For a surface coverage of 2/3 of a monolayer, the Cu adatoms are known to form hexagons on Au(111), in the center of which sulfate ions are coadsorbed.<sup>12,13</sup> These sulfate ions are amazingly easily imaged by STM and are indeed seen to arrange in a hexagonal ( $\sqrt{3} \times \sqrt{3}$ ) R30° structure with a next-

neighbor distance of 4.9 Å (Fig. 2). The reason for this unusual behavior—anions will not normally sit still—is that the anions are immobilized by the honeycomb structure of the underlying Cu adatoms; the Cu hexagons act as two-dimensional cages for the sulfate ions.<sup>14,15</sup> We stress the fact that for any surface species (adion, adatom or admolecule) immobilization is a basic prerequisite for imaging by STM. Such immobilization is normally achieved by the formation of ordered adlayers (so-called superstructures).

As the electrode potential is driven more negative, the Cu adatoms form a complete monolayer at about + 80 mV vs. Cu/Cu<sup>2+</sup>. This monolayer is pseudomorphic, i.e. has the same lattice parameters as the underlying gold surface. The Cu adatoms reside in the 3-fold hollow sites of the substrate, resulting in a 13% strained Cu layer. It is this strain which causes 3-dimensional cluster growth from the very beginning of overpotential (bulk) deposition.

Pseudomorphic growth is possible only when the adatoms are smaller

than the substrate atoms. In the reverse case, for example, for Pb on Ag(111), the adatoms no longer fit in every lattice site. In that case a full monolayer is reached by a hexagonal-close-packed (hcp) structure, in which the Pb adatoms acquire the next-neighbor distance of bulk lead<sup>16</sup> (Fig. 3). Since the Pb adatoms are no longer in registry with the substrate, their positions result in different heights (the lowest position is the 3-fold hollow site, the highest the on-top position) which leads to a long-range corrugation (so-called Moiré pattern, as shown in Fig. 3), clearly visible in STM images.

### Bulk Deposition

It has been well-known now for many decades that at low or moderate overpotentials bulk deposition predominantly starts at surface defects, which act as nucleation centers for the new phase. Even model systems consisting of monocrystalline surfaces have plenty of imperfections; minor defects will be in the form of monatomic high steps or screw dislocations and major defects

will result from massive step bunching at grain boundaries.

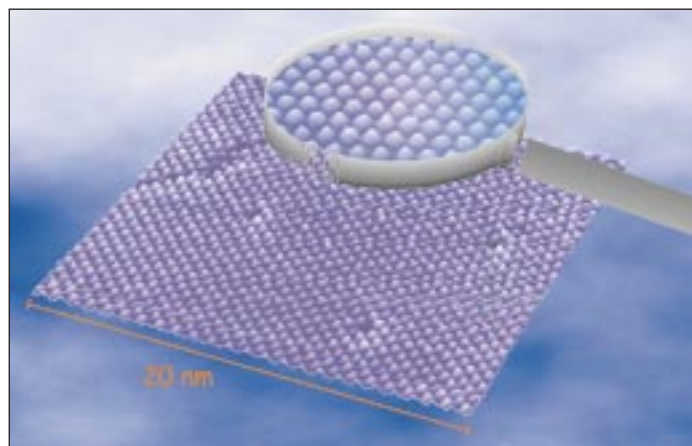
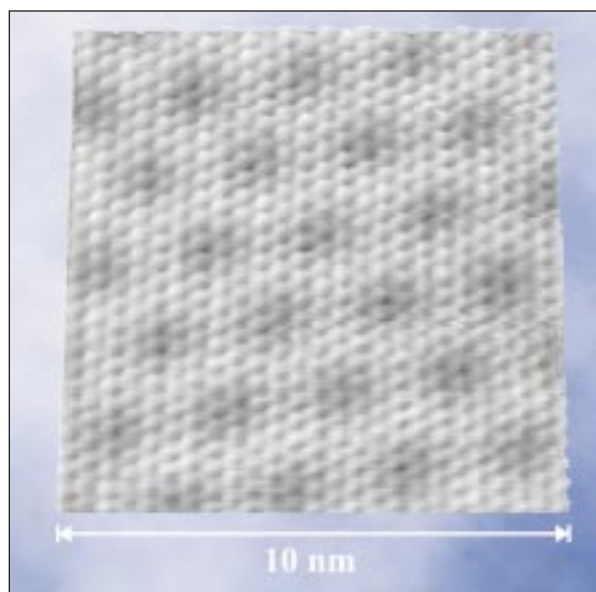
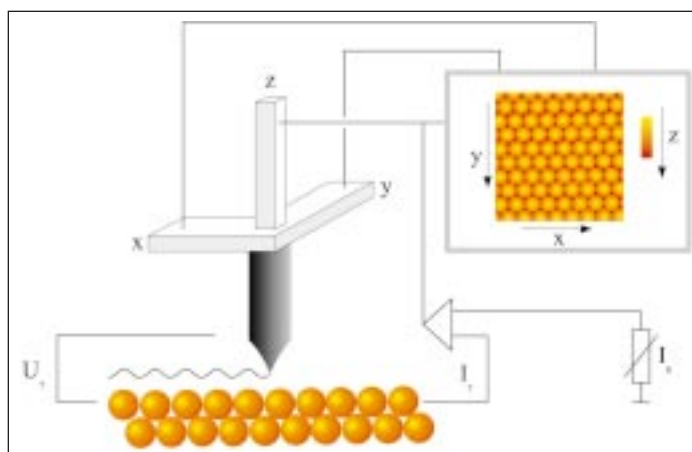
Hence, the number of surface defects and their spatial distribution will have a marked impact on the topography of the growing overlayer.<sup>17</sup> Obviously, this applies particularly to films of nanometer thickness which are receiving increasing attention. One of the unequalled virtues of STM, in contrast to other surface techniques which either integrate over the whole electrode area or yield information in reciprocal space, is the ability to obtain detailed information about the spatial distribution of irregularities and defects on surfaces.

The strong influence of surface defects on the nucleation-and-growth behavior of Cu is demonstrated in Fig. 4, where deposition onto Au(111) (which is already covered by a Cu UPD monolayer) is seen to occur exclusively at the monatomic high steps of the substrate. The growing Cu clusters virtually decorate the surface defects of the substrate, whereas the flat terraces remain uncovered for a relatively long time. Such behavior leads to inhomogeneous

Fig. 1. (top, right) Operating principle of the scanning tunneling microscope. If a sharp metal tip and a conducting surface are approached to sufficient proximity, an applied voltage between those two leads to a tunneling current, which sensitively depends on the tip-sample distance. Topographic information is obtained by scanning the tip across the surface.

Fig. 2. (below, right) STM image (20 x 20 nm<sup>2</sup>) of the copper/sulfate coadsorption structure on Au(111) in 0.1 M H<sub>2</sub>SO<sub>4</sub> + 1mM CuSO<sub>4</sub> at 0.15 V vs. Cu/Cu<sup>2+</sup>. Solely the sulfate anions forming a (√3 x √3) R30° superstructure are perceived by STM.

Fig. 3. (below) Moiré pattern formed by an underpotentially deposited Pb monolayer on Ag(111) in the presence of citrate at -440 mV vs. SCE, 0.5 M NaClO<sub>4</sub> + 0.1 M Na<sub>2</sub>Hcit + 1mM Pb (NO<sub>3</sub>)<sub>2</sub>. From Ref. 33.



geneous film thicknesses and rough overlayers. The remedy for this and other modes of undesirable growth—the use of additives—has been known to the plating industry for a long time.

### Additives

In industrial plating baths, so-called levelers and brighteners are added to favorably modify the nucleation and/or growth behavior to produce uniform metal films.<sup>18,19</sup> Several classes of such additives are known, many of them being organic molecules that interact strongly with the metal surface and others are anionic complexing agents. A number of mechanisms has been formulated for their influence on metal growth. Nevertheless, the majority of patented (usually many-compound) plating baths is the product of empirical research and it

may be fair to say that the action (and interaction) of plating agents is still far from being fully understood on a molecular basis. One classical additive is the dye *crystal violet* (hexamethyl-pyrosanilinium chloride) and its action is demonstrated in Fig. 5. Addition of crystal violet causes a quasi-two-dimensional growth despite the fact that nucleation still occurs at step edges.<sup>7,20</sup> However, the growth rate normal to the surface is strongly reduced (most likely due to the dye adsorbing at the flat tops of the Cu clusters) allowing the lateral spread of the deposit to become dominant. The 3-dimensional cluster growth in the absence of any additive which leads to a rough overlayer is shown in Fig. 5 for comparison. Another example of a deposit being influenced by the presence of an additive is seen in Fig. 6. The presence of the surfactant sodium dodecylsulfate in the solution was

shown to inhibit nucleation on terraces even at high overpotentials and thus, to favor the growth of a few large, well-defined copper crystals.<sup>21</sup> Atomic force microscopy, a technique closely related to STM, has also been successfully used to monitor additive influence on metal deposition processes.<sup>22</sup> Although STM studies on that topic are only beginning, it is easily foreseen that this technique will significantly enhance our understanding of how organic additives control the deposition process.

### Epitaxial Growth

For metal deposition onto a foreign (monocrystalline) metal substrate it is commonly observed that only the first monolayer acquires the lattice parameters of the substrate, that is if pseudomorphic growth occurs at all. Because of the increasing strain from the formation

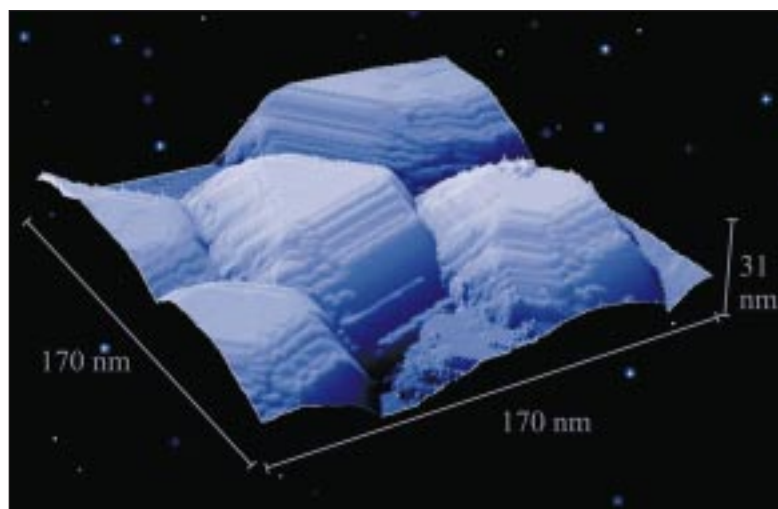
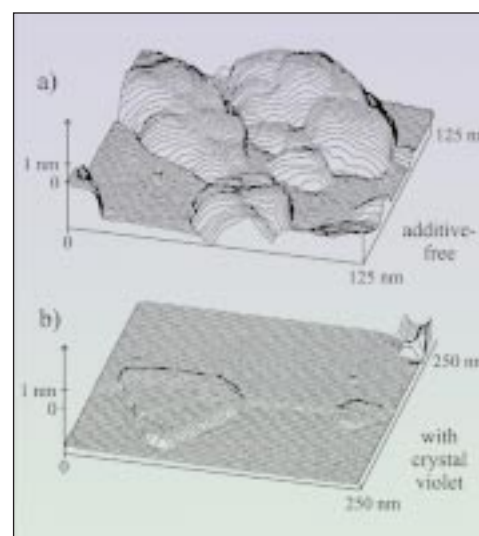
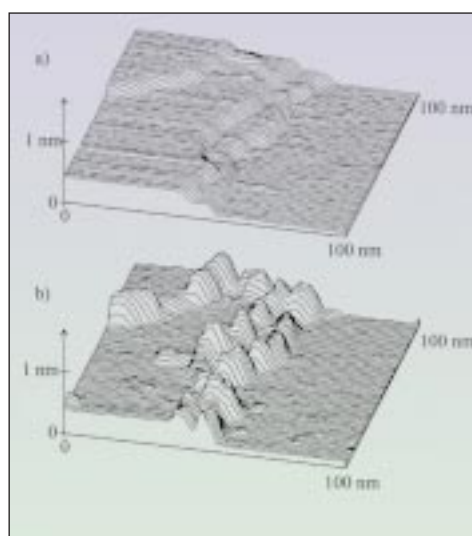


FIG. 4. (above, left) STM images of Au(111) in 5 mM  $H_2SO_4$  + 0.05 mM  $CuSO_4$  at (a) +0.40 V and (b) -0.20 V vs.  $Cu/Cu^{2+}$ . Preferential nucleation of Cu clusters at defects of the Au(111) electrode leads to step decoration. From Ref. 7.

FIG. 5. (above, right) The initial stages of Cu deposition on Au(111) (a) in the absence of organic additive and (b) in the presence of crystal violet (CV). (a)  $E = -0.15$  V, 5 mM  $H_2SO_4$  + 0.05 mM  $CuSO_4$ . (b)  $E = -0.13$  V, 0.05 M  $H_2SO_4$  + 1 mM  $CuSO_4$  + 0.1 mM CV. All potentials vs.  $Cu/Cu^{2+}$ . From Ref. 7.

FIG. 6. (left) Cu crystallites deposited on Au(111) in the presence of sodium dodecyl sulfate, 0.05 M  $H_2SO_4$  +  $5 \times 10^{-4}$  M  $CuSO_4$  +  $10^{-4}$  M SDS after 20 min deposition at -0.17 V vs.  $Cu/Cu^{2+}$ . From Ref. 21.

of pseudomorphic multilayers, the deposit then continues to grow in its own habit beyond the first monolayer. Exceptions to this rule have been reported for Cu on Ag(111)<sup>23</sup> and Pd on Au(111),<sup>24</sup> where two monolayers are believed to grow pseudomorphically.

With Ag(100) and Au(100) as substrates, however, STM studies have revealed the growth of several pseudomorphic layers of Cu.<sup>25,26</sup> What appears to be unbelievable at first (the lattice mismatch of both amounts to 13%) is due to a substrate-induced change of the Cu-structure from face-centered cubic (fcc) to body-centered cubic (bcc). Although fcc Cu is the most thermodynamically stable crystal structure, bcc Cu, which is energetically less favorable by only a relatively small amount of 20 meV, has the advantage of a negligible lattice misfit with Ag(100) or Au(100). This almost perfect lattice match between bcc Cu and the (100) face of Ag or Au seems to over-

compensate the energy difference between the two Cu modifications and allows bcc Cu to grow. Systematic studies have revealed that exactly eight layers of bcc Cu can be grown onto Ag(100) and 10 layers onto Au(100).

With the 9<sup>th</sup> and 11<sup>th</sup> layer, respectively, a structural transition suddenly takes place which causes the Cu surface to become buckled (Fig. 7). The emerging new surface structure shows small domains rotated by 90° from each other, thus revealing the substrate's twofold symmetry. The atomic structure leading to those stripes is not yet completely solved, but has been considered to be the beginning of a structural transition toward fcc.<sup>25,26</sup> The striped structure, although it gradually deteriorates with increasing film thickness, was observed for many layers until crystallites with presumably pure fcc structure emerged. The most striking feature of the bcc Cu overlayer and the sudden transition to the buckled phase was

revealed by in situ surface x-ray diffraction (SXRD).<sup>27</sup> The transition appears to be fully reversible. For Au(100), for example, all ten bcc Cu layers switch to the buckled phase with deposition of the 11<sup>th</sup> layer. Likewise, dissolution of the 11<sup>th</sup> Cu layer on Au(100) transforms the first ten Cu layers back into bcc Cu. A second interesting, yet unexplained observation may be worth pointing out again. This is the difference in the maximum bcc Cu film thickness for Ag(100) and Au(100) which is invariably eight and ten layers, respectively. From the 9<sup>th</sup> and the 11<sup>th</sup> layer onward, the surface is buckled. Clearly, such detailed structure information about Cu overlayers would not have been possible without the use of an STM.

### Nanostructuring

For several years now it has been demonstrated by various groups that the scanning tunneling microscope is

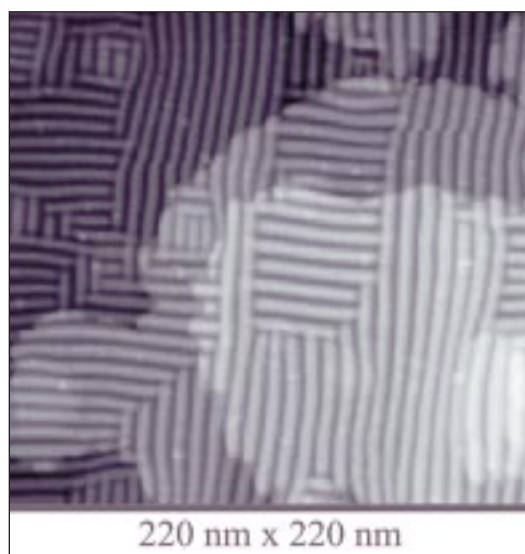


FIG. 7. (above) Striped structure of the 11<sup>th</sup> Cu layer observed with the STM during copper deposition on Au(100). The reason for this phenomenon is the structural transition that the ten layers of bcc Cu undergo with deposition of the 11<sup>th</sup> layer.  $E = -0.2$  V,  $0.1$  M  $H_2SO_4 + 0.5$  mM  $CuSO_4$ . From Ref. 26.

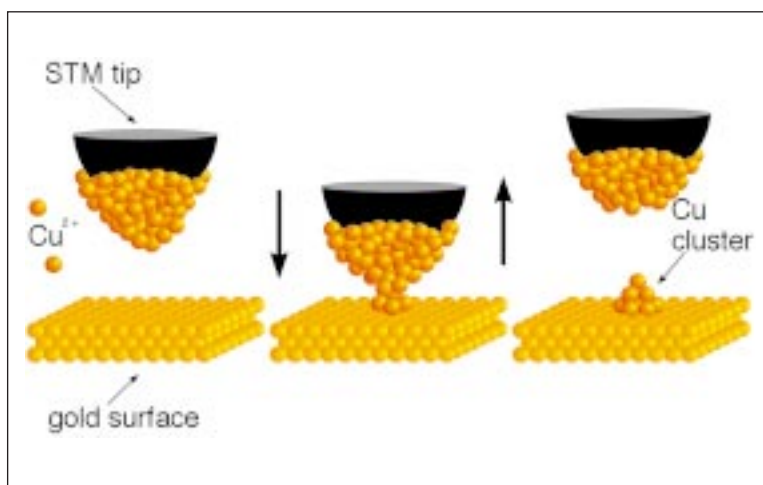
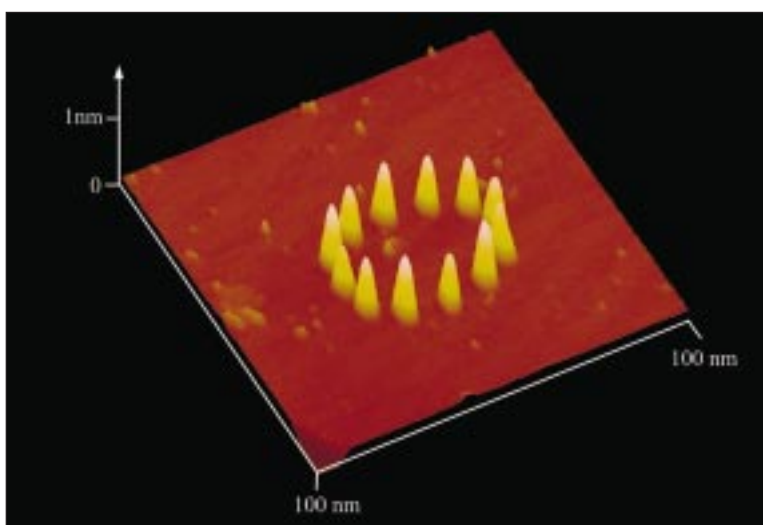


FIG. 8. (above, right) Principle of tip-induced metal deposition: copper is electrochemically deposited on the tip. Approach of the tip to the surface leads to a jump-to-contact, accompanied by the formation of a connective neck. Withdrawal of the tip causes the connective neck to break which leaves a small copper cluster on the surface.

FIG. 9. (right) A circle of twelve Cu clusters formed on Au(111) by the method schematically depicted in Fig. 8 with  $0.05$  M  $H_2SO_4 + 1$  mM  $CuSO_4$ ,  $E = +10$  mV vs.  $Cu/Cu^{2+}$ . The clusters have a height of about  $0.8$  nm and show a full width at half maximum of about  $3.5$  nm; the circle has a diameter of  $41$  nm. From Ref. 29.



not only a powerful tool for imaging electrode surfaces in real space and with atomic resolution, it can also be used for structuring surfaces on an atomic scale.<sup>28</sup> One of several possible methods for generating small metal clusters at predetermined positions is schematically depicted in Fig. 8.<sup>29,30</sup> Metal is electrochemically deposited onto the uncoated part of the tip. Then the tip is made to approach the surface in a controlled fashion until a so-called "jump-to-contact" occurs with the formation of a connective neck between tip and sample surface.<sup>31</sup> When the tip is withdrawn, the connective neck breaks and a small cluster of metal remains on the surface. The material on the tip is continuously replenished, simply by keeping the tip potential sufficiently negative, thus offering the possibility of depositing a large number of clusters without exhausting the supply. The clusters have been found to be surprisingly stable against anodic dissolution.<sup>30</sup> The process was first developed and successfully realized for the system Cu/Au(111) in sulfuric acid solution (in this case, the Cu clusters were in fact deposited on top of the Cu UPD monolayer), but has since been accomplished with a number of other substrate and deposit metals.<sup>30</sup> A circle of twelve copper clusters assembled on a Au(111) surface by the aforementioned technique is shown in Fig. 9. The clusters have an average height of 0.8 nm.

This process of tip-induced metal deposition has meanwhile been automated with the help of microprocessors, which control the x-, y- and z-motions of the tip and allow cluster generation at a speed of 50-80 Hz. Likewise, the creation of more or less complex patterns of clusters is fully automated.<sup>29</sup>

Future applications of this technique include the generation of metal nanowires on semiconductors, as well as the study of electrochemical reactions at cluster fields of electrocatalytically active material. For the latter purpose, the creation of very large arrays of clusters seems necessary in order to detect reactions on the clusters. To demonstrate that large arrays can indeed be produced within a reasonably short time, a field of 10,000 clusters was recently created within several minutes.<sup>32</sup> Moreover this proves how fast the tip is loaded again with copper from solution, so that an almost unending reservoir of material is available for surface modification.

## Conclusion

The invention of scanning tunneling microscopy has opened up unique views of the initial stages of metal deposition in real space and real time on the nanometer scale as shown by the few selected examples. It has enabled electrochemists to monitor topographical changes associated with the deposition process, characterize surfaces on an atomic level, and discover surface phenomena which might have eluded other techniques. ■

## References

1. E. Budevski, G. Staikov, and W. J. Lorenz, *Electrochemical Phase Formation and Growth*, VCH, Weinheim (1996).
2. B. Scharifker and G. Hills, *Electrochim. Acta*, **28**, 879 (1983).
3. D. M. Kolb, *Ber. Bunsen-Ges. Phys. Chem.*, **77**, 891 (1973).
4. R. Lacmann and H.-J. Randig, *J. Crystal Growth*, **17**, 97 (1972).
5. *Nanoscale Probes of the Solid/Liquid Interface*, A. A. Gewirth and H. Siegenthaler, Editors, NATO ASI Vol. E288, Kluwer, Dordrecht (1995).
6. K. Itaya, *Prog. Surf. Sci.*, **58**, 121 (1998).
7. T. Will, M. Dietterle, and D. M. Kolb, in *Nanoscale Probes of the Solid/Liquid Interface*, A. A. Gewirth and H. Siegenthaler, Editors, NATO ASI Vol. E288, 37, Kluwer, Dordrecht (1995).
8. C. E. Bach, R. J. Nichols, W. Beckmann, H. Meyer, A. Schulte, J. D. Besenhard, and P. D. Jannakoudakis, *J. Electrochem. Soc.*, **140**, 1281 (1993).
9. D. M. Kolb, *Advances in Electrochemistry and Electrochemical Engineering*, H. Gerischer, and C. W. Tobias, Editors, Vol. 11, 125, Wiley, New York (1978).
10. J. W. Schultze and D. Dickertmann, *Surf. Sci.*, **54**, 489, (1976).
11. K. Jüttner and W. J. Lorenz, *Z. Phys. Chem. NF*, **122**, 136 (1980).
12. D. M. Kolb, *Ber. Bunsen-Ges. Phys. Chem.*, **92**, 1175 (1988).
13. M. F. Toney, J. N. Howard, J. Richer, G. L. Borges, J. G. Gordon, O. R. Melroy, D. Yee, and L. B. Sorensen, *Phys. Rev. Lett.*, **75**, 4472 (1995).
14. D. A. Huckaby and L. Blum, *J. Electroanal. Chem.*, **315**, 255 (1991).
15. L. Blum, M. Legault, and P. Turq, *J. Electroanal. Chem.*, **379**, 35 (1994).
16. M. G. Samant, M. F. Toney, G. L. Borges, L. Blum, and O. R. Melroy, *J. Phys. Chem.*, **92**, 220 (1988).
17. K. Sieradzki, N. Dimitrov, and S. Brankovic, Abstract No. 520, The Electrochemical Society Meeting Abstracts, Vol. 98-2, Boston, MA, Nov. 1-6, 1998.
18. H. Fischer, *Elektrolytische Abscheidung und Elektrokristallisation von Metallen*, Springer, Berlin (1954).
19. T. C. Franklin, *Plat. Surf. Fin.*, **81**, 62 (1994).
20. R. J. Nichols, C. E. Bach, and H. Meyer, *Ber. Bunsen-Ges. Phys. Chem.*, **97**, 1012 (1993).
21. M. Petri, Diploma Thesis, University of Ulm, Germany (1998).

22. E. D. Eliadis and R. C. Alkire, *J. Electrochem. Soc.*, **145**, 1218 (1998).
23. M. Dietterle, T. Will, and D. M. Kolb, *Surf. Sci.*, **342**, 29 (1995).
24. M. Baldauf and D. M. Kolb, *J. Phys. Chem.*, **100**, 11375 (1996).
25. M. Dietterle, T. Will, and D. M. Kolb, *Surf. Sci.*, **396**, 189 (1998).
26. R. J. Randler, M. Dietterle, and D. M. Kolb, *Z. Phys. Chem.*, **208**, 43 (1999).
27. R. J. Randler, D. M. Kolb, B. M. Ocko, and I. K. Robinson, in preparation.
28. W. Li, J. A. Virtanen, and R. M. Penner, *Appl. Phys. Lett.*, **60**, 1181 (1992).
29. D. M. Kolb, R. Ullmann, and T. Will, *Science*, **275**, 1097, (1997).
30. D. M. Kolb, R. Ullmann, and J. C. Ziegler, *Electrochim. Acta.*, **43**, 2751 (1998).
31. U. Landman and W. D. Luetke, *Springer Ser. Surf. Sci.*, **29**, 207 (1993).
32. G. E. Engelmann, J. C. Ziegler, and D. M. Kolb, *Surf. Sci.*, **401**, L420 (1998).
33. M. H. Hölzle, PhD Thesis, University of Ulm, Germany (1995).

## About the Authors

**D. M. Kolb** is a full professor and head of the Electrochemistry Department at the University of Ulm. His research deals amongst others with the fundamental aspects of metal deposition.

**M. A. Schneeweiss** is a senior scientist at the Department of Electrochemistry, University of Ulm. She is currently engaged in the study of chemically modified electrodes and their possible application in metal deposition.